Vibrational Excitation in Products of Nucleophilic Substitution: The Dissociation of Metastable $X^-(CH_3Y)$ in the Gas Phase

Susan T. Graul*,† and Michael T. Bowers*,‡

Contribution from the Department of Chemistry, Carnegie Mellon University, Pittsburgh, Pennsylvania 15213, and Department of Chemistry, University of California, Santa Barbara, California 93106

Received November 29, 1993®

Abstract: The relative kinetic energy distributions for the $Y^- + CH_3X$ nucleophilic substitution products from dissociation of metastable $X^-(CH_3Y)$ (X = Cl, Br; Y = Br, I) have been analyzed by means of ion kinetic energy spectroscopy, and the results modeled using statistical phase space theory. Comparison of the experimental distributions with the theoretical distributions predicted for statistical partitioning of the available energy reveals that the substitution products are translationally cold. The theoretically calculated distributions can be made to agree with experiment if most of the energy released in the dissociation is assumed to be unavailable for randomization, such that it cannot partition to relative translation. This unavailable energy must correspond to internal energy, most likely vibrational excitation, in the CH_3X products. These results are consistent with recent theoretical predictions of non-RRKM dynamics in gas-phase S_N2 reactions.

Introduction

Probably the most widely used model for thermal energy gas-phase ion reaction dynamics is that given by statistical theories, in particular RRKM and statistical phase space theory.[1-4] The keystone of the statistical model for bimolecular and unimolecular ion chemistry is the assumption that internal energy is randomized among all available modes in the reacting or dissociating species and therefore that the kinetics of the reaction and the deposition of the reaction energy are determined purely by densities of internal states (subject to energy and angular momentum conservation). This conceptually simple yet informative model of ion reactions can provide qualitative and quantitative information about the potential energy surface that controls the reaction, such as the natures of rate-limiting transition states and the thermochemistry of the reaction. The assumption of statistical reaction dynamics is implicit in the common use of reaction kinetics, bracketing methods, and appearance potentials to estimate reaction thermochemistry.

Through extensive experimental investigations and RRKM statistical theoretical modeling, Brauman and co-workers have demonstrated that the kinetics of gas-phase nucleophilic substitution reactions can be rationalized in terms of a double-well potential for the reaction coordinate (Figure 1).[5-9] Such a potential had been found earlier in ab initio molecular orbital studies of S_N2 reactions[10-12] and has since been confirmed

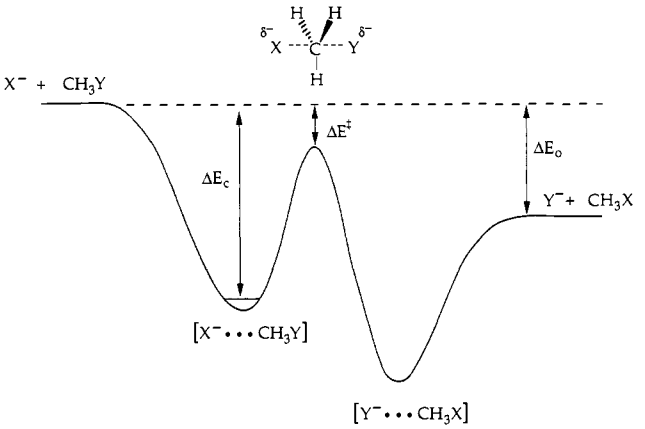

Figure 1. Schematic double-well potential for an unsymmetrical gas-phase bimolecular nucleophilic substitution reaction involving methyl halides.

theoretically and experimentally for numerous other S_N2 reactions.[13-20] These important studies laid the foundation for more recent detailed examinations of S_N2 reaction dynamics that have added an interesting twist to the picture; results of a number of theoretical studies have indicated *non*-RRKM dynamics for certain nucleophilic substitution reactions, both in solution and in the gas phase.[21-26] For example, theoretical trajectory calculations for the $Cl^- + CH_3Cl$ reaction in the gas phase indicate such non-RRKM behavior as vibrational state-specific rate enhancement of a direct substitution reaction, decoupling of vibrational modes in the transient S_N2 reaction intermediate,

† Carnegie Mellon University.
‡ University of California.
® Abstract published in *Advance ACS Abstracts*, April 1, 1994.

(1) Forst, W. *Theory of Unimolecular Reactions*; Academic Press: New York, 1973.
(2) Robinson, P. J.; Holbrook, K. A. *Unimolecular Reactions*; Wiley-Interscience: New York, 1972.
(3) Pechukas, P. In *Dynamics of Molecular Collisions, Part B*; Miller, W. H.; Ed.; Plenum Press: New York, 1976.
(4) Chesnavich, W. J.; Bowers, M. T. In *Gas Phase Ion Chemistry*; Bowers, M. T.; Ed.; Academic Press: New York, 1979; Vol. 1, pp 119.
(5) Lieder, C. A.; Brauman, J. I. *J. Am. Chem. Soc.* **1974**, *96*, 4029.
(6) Brauman, J. I.; Olmstead, W. N.; Lieder, C. A. *J. Am. Chem. Soc.* **1974**, *96*, 4030.
(7) Olmstead, W. N.; Brauman, J. I. *J. Am. Chem. Soc.* **1977**, *99*, 4219.
(8) Asubiojo, O. I.; Brauman, J. I. *J. Am. Chem. Soc.* **1979**, *101*, 3715.
(9) Pellerite, M. J.; Brauman, J. I. *J. Am. Chem. Soc.* **1980**, *102*, 5992.
(10) Dedieu, A.; Veillard, A. In *Quantum Theory of Chemical Reactions*; Daudel, R.; Pullman, A.; Salem, L.; Veillard, A.; Eds.; Reidel Publishers: New York, 1979; Vol. 1, pp 69.
(11) Dedieu, A.; Veillard, A. *Chem. Phys. Lett.* **1970**, *5*, 328.
(12) Dedieu, A.; Veillard, A. *J. Am. Chem. Soc.* **1972**, *94*, 6730.
(13) Wolfe, S.; Mitchell, D. J.; Schlegel, H. B. *J. Am. Chem. Soc.* **1981**, *103*, 7692.
(14) Chandrasekhar, J.; Smith, S. F.; Jorgensen, W. L. *J. Am. Chem. Soc.* **1985**, *107*, 154.
(15) Tucker, S. C.; Truhlar, D. G. *J. Am. Chem. Soc.* **1990**, *112*, 3338.
(16) Shi, Z.; Boyd, R. J. *J. Am. Chem. Soc.* **1990**, *112*, 6789.
(17) Vande Linde, S. R.; Hase, W. L. *J. Phys. Chem.* **1990**, *94*, 2778.
(18) Graul, S. T.; Bowers, M. T. *J. Am. Chem. Soc.* **1991**, *113*, 9696.
(19) Cyr, D. M.; Posey, L. A.; Bishea, G. A.; Han, C.-C.; Johnson, M. A. *J. Am. Chem. Soc.* **1991**, *113*, 9697.
(20) Wilbur, J. L.; Brauman, J. I. *J. Am. Chem. Soc.* **1991**, *113*, 9699.
(21) Basilevsky, M. V.; Ryaboy, V. M. *Chem. Phys. Lett.* **1986**, *129*, 71.

0002-7863/94/1516-3875$04.50/0 © 1994 American Chemical Society

and multiple crossings for the transition state dividing surface.[23-25,27] Theoretical studies have also shown, along with other nonstatistical dynamics, vibrational excitation in the substitution products for $X^- + CH_3F$, where X = H, F, OH.[21] Recent experimental work on the $Cl^- + CH_3Br$ reaction revealed that energy made available to the reaction as relative translational energy of the reactants had a different effect on reaction kinetics compared to changes in the internal energy of CH_3Br.[28] That result could be indicative of decoupled vibrational modes in the intermediate complex[24,25] and raises the question of whether statistical theory can be applied in a meaningful way to gas-phase S_N2 reactions. If these nonstatistical dynamics prove to be general for S_N2 reactions, the implications could be far-reaching for our understanding of gas-phase ion chemistry, a field in which RRKM and related statistical theories have been invoked extensively in interpretative and diagnostic capacities.

Examination of the energy deposition in the products of ion–molecule reactions can reveal useful information about the reaction dynamics. One general and sensitive method of probing energy deposition involves monitoring the kinetic energies of the product ions.[29-32] This method was utilized in a kinetic energy–ion cyclotron resonance (KE–ICR) study of the $F^- + CH_3Cl$ reaction, which displayed nonstatistical energy partitioning and translationally hot products.[33] Our own results, described herein and communicated previously in preliminary form,[18] differ dramatically from the KE–ICR results. We have examined the relative kinetic energy distributions for the substitution products from decomposition of metastable $X^-(CH_3Y)$ adduct species to $Y^- + CH_3X$, where X = Cl or Br and Y = Br or I. These adduct species are treated as models for the intermediates in the bimolecular reaction (eq 1).

$$X^- + CH_3Y \rightleftarrows [X^-(CH_3Y)]^* \rightarrow Y^- + CH_3X \qquad (1)$$

The partitioning of the available energy between internal and relative translational energy of the Y^- and CH_3X products has been modeled using statistical phase space theory.[4,34] Comparison of the calculated relative kinetic energy distributions with the experimental distributions indicates that a much smaller amount of the available energy is released to relative translation than is predicted for a statistical process. In this article, we describe our experimental results and the phase space calculations and discuss our results in the context of other theoretical and experimental studies of S_N2 reaction dynamics.

Experimental Section

These experiments were carried out in a reverse-geometry sector mass spectrometer (V. G. Analytical ZAB-2F). The Cl^- and Br^- ions were generated in a temperature- and pressure-variable ion source by electron attachment to CCl_4 and CH_2Br_2, respectively. The $X^-(CH_3Y)$ adducts were then formed by association reactions in the ion source with the pressure of methyl halide gas maintained as low as practical to minimize the number of stabilizing collisions. The methyl halide pressures were typically 0.05–0.1 Torr, and the source temperature 20–50 °C. At these pressures, the collision frequency is approximately $10^6\ s^{-1}$. The $X^-(CH_3Y)$ adducts could be detected only for source pressures above about 0.05 Torr. Detection of ions formed in the ion source of the ZAB requires ion lifetimes of 10 μs or longer, which corresponds to the total time required for the ion to traverse the instrument flight path to the detector. Ions that undergo unimolecular dissociation in the second-field-free region of the mass spectrometer are termed "metastable" ions.[35]

The products from metastable $X^-(CH_3Y)$ dissociations occurring in the second field-free region of the ZAB-2F were energy-analyzed at the electrostatic sector. The resulting laboratory energy distributions were converted to product relative kinetic energy distributions by a transformation of coordinates.[36] Collisional activation studies were carried out by leaking helium into the collision cell located in the second field-free region. The dependence of the distributions on ion source pressure was examined by comparing distributions measured at the lowest ion source pressures at which metastable dissociation was detectable (about 0.05 Torr) to distributions measured for source pressures of about 0.2–0.3 Torr.

The bimolecular kinetics for these reactions have been measured by Gronert et al.[37] Here we model those results with statistical phase space theory in order to estimate activation energies. The resulting values are used in an integrated model of the dissociation process in which the effects of the S_N2 transition state on the final product kinetic energy distribution are considered. The calculations and the parameters used are described in the Appendix.

To fit the experimental KERDs with the distributions calculated for internally excited products, we calculated a series of distributions assuming 0–100% of the reaction energy was unavailable for randomization. Weighted sums of these distributions were fit to the experimental data using a least-squares routine, and the best fits were taken as those with minimal residual errors. Adequate fits were obtained in each case with combinations of three calculated distributions.

Results

In these experiments, the $X^-(CH_3Y)$ adduct species could be detected only for ion source pressures in excess of about 0.05 Torr, which corresponds to a collision frequency of about $10^6\ s^{-1}$. The requirement for relatively high source pressures to generate long-lived $X^-(CH_3Y)$ adducts may arise from the need to "cool" the reactant X^- ions, which are probably generated with hyperthermal kinetic energies by the dissociative attachment reactions. Under these conditions, the adducts may experience stabilizing collisions, in which case the nascent internal energy and angular momentum distributions of the collision complexes may be altered significantly. However, the probability of the transient adducts experiencing collisional stabilization is low, due to their relatively short source residence times. In any case, the experimental results indicate that some fraction of the adducts exits the ion source with adequate internal energy to dissociate on the metastable time scale, and the metastable dissociation experiment probes only these "chemically activated" adducts.

Metastable Dissociation and Collisional Activation. The S_N2 reaction coordinate has two potential wells, corresponding to two isomeric forms of the ion–molecule complex (Figure 1). For the remainder of this article, we will refer to the reactant complex as $X^-(CH_3Y)$ and the product complex as $Y^-(CH_3X)$ with the convention that the reactant complex is the higher energy isomer. Our experiment is designed to probe the metastable dissociation of the reactant complex on the 10^{-5} s time scale. Because the ion formation step was carried out under multiple-collision conditions, there is some possibility that the reactant complexes that undergo the substitution reaction in the ion source might be trapped in

(22) Bergsma, J. P.; Gertner, B. J.; Wilson, K. R.; Hynes, J. T. *J. Chem. Phys.* **1987**, *86*, 1356.
(23) Vande Linde, S. R.; Hase, W. L. *J. Am. Chem. Soc.* **1989**, *111*, 2349.
(24) Vande Linde, S. R.; Hase, W. L. *J. Phys. Chem.* **1990**, *94*, 6148.
(25) Vande Linde, S. R.; Hase, W. L. *J. Chem. Phys.* **1990**, *93*, 7962.
(26) Gertner, B. J.; Whitnell, R. M.; Wilson, K. R.; Hynes, J. T. *J. Am. Chem. Soc.* **1991**, *113*, 74.
(27) Cho, Y. J.; Vande Linde, S. G.; Zhu, L.; Hase, W. L. *J. Chem. Phys.* **1992**, *96*, 8275.
(28) Viggiano, A. A.; Morris, R. A.; Paschekewitz, J. S.; Paulson, J. F. *J. Am. Chem. Soc.* **1992**, *114*, 10477.
(29) Beynon, J. H.; Caprioli, R. M.; Ast, T. *Org. Mass Spectrom.* **1971**, *5*, 229.
(30) Beynon, J. H.; Fontaine, A. E.; Lester, G. R. *Int. J. Mass Spectrom. Ion Phys.* **1972**, *8*, 341.
(31) Terwilliger, D. T.; Elder, J. J. F.; Beynon, J. H.; Cooks, R. G. *Int. J. Mass Spectrom. Ion Phys.* **1975**, *16*, 225.
(32) Mauclaire, G.; Derai, R.; Fenistein, S.; Marx, R. *J. Chem. Phys.* **1979**, *70*, 4017.
(33) VanOrden, S. L.; Pope, R. M.; Buckner, S. W. *Org. Mass Spectrom.* **1991**, *26*, 1003.
(34) Chesnavich, W. J.; Bowers, M. T. *Prog. React. Kinetics* **1982**, *11*, 137.
(35) Cooks, R. G.; Beynon, J. H.; Caprioli, R. M.; Lester, G. R. *Metastable Ions*; Elsevier: Amsterdam, 1973.
(36) Jarrold, M. F.; Illies, A. J.; Kerchner, N. J.; Wagner-Redeker, W.; Bowers, M. T.; Mandich, M. L.; Beauchamp, J. L. *J. Phys. Chem.* **1983**, *87*, 2213.
(37) Gronert, S.; DePuy, C. H.; Bierbaum, V. M. *J. Am. Chem. Soc.* **1991**, *113*, 4009.

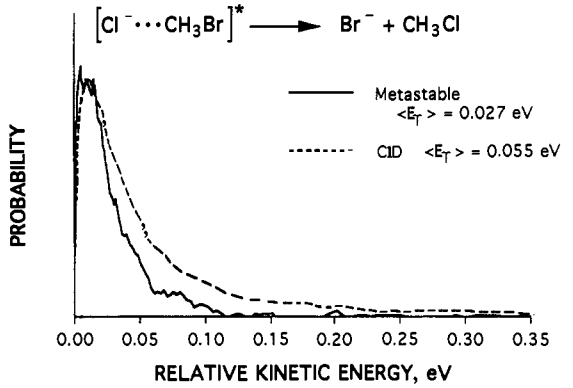

Figure 2. Experimental kinetic energy release distributions for the displacement reaction $Cl^-(CH_3Br) \rightarrow Br^- + CH_3Cl$ under metastable (solid line) and collisionally activated (dashed line) conditions.

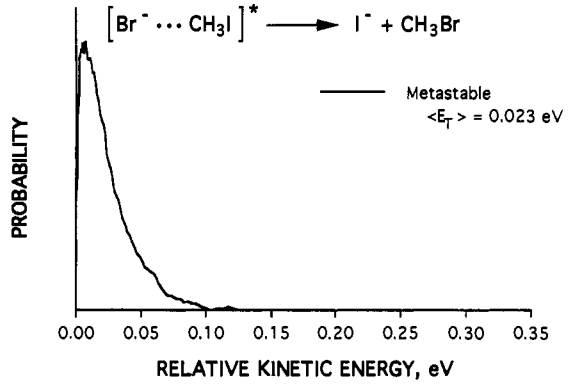

Figure 3. Experimental metastable kinetic energy release distribution for the displacement reaction $Br^-(CH_3I) \rightarrow I^- + CH_3Br$.

the potential energy well on the product side and exit the source as the isomeric product complex. In order to determine whether the $X^-(CH_3Y)$ population is contaminated by the product complex $Y^-(CH_3X)$, we generated in separate experiments the product complexes and studied the spontaneous and collisionally activated dissociation of theese ions, as observed without and with helium target gas added to the collision cell in the second field-free region, respectively.

The major fragment ion formed by metastable dissociation of $Cl^-(CH_3Br)$ was the Br^- product of the displacement reaction (eq 2). The kinetic energy release distribution (KERD) for the $Br^- + CH_3Cl$ products is shown in Figure 2; the average kinetic energy for this distribution is approximately 27 meV. The average kinetic energy releases for these metastable dissociation products were weakly dependent on ion source pressure but varied by only about ±3 meV over the accessible pressure range. Also shown in Figure 2 is the KERD obtained for $Br^- + CH_3Cl$ products from collisional activation of the $Cl^-(CH_3Br)$ adduct using helium target gas and an ion kinetic energy of 8 keV (collision energy of 240 eV). The two distributions are clearly different, verifying that we observe metastable dissociation in the second field-free region.

$$Cl^- + CH_3Br \underset{k_b}{\rightleftarrows} [Cl^-(CH_3Br)]^* \xrightarrow{k_r} Br^- + CH_3Cl \qquad (2)$$

The Cl^- fragment ion that results from cleavage of the electrostatic bond (back-dissociation in eq 2) is barely detectable in the metastable ion spectrum and constitutes less than 1% of the total product ion intensity. Except for a much lower signal-to-noise ratio, the KERD for the $Cl^- + CH_3Br$ products in the experiments conducted without added collision gas is essentially the same as the KERD for the collisionally activated process, with average relative kinetic energies of the products of 55–60 meV. This result suggests that the weak Cl^- signal in the metastable experiments arises primarily from collisional activation by residual background gas. It is interesting to note that the bimolecular reaction leads to $Br^- + CH_3Cl$ only in one out of a hundred collisions,[37] which corresponds to a branching ratio for dissociation of the intermediate complex of $k_f/(k_f + k_b) = 0.01$, in contrast to the metastable branching ratio of $k_f/(k_f + k_b)$ of about 1. The remarkable difference in the branching ratio for the metastable dissociation as compared to the efficiency of the bimolecular reaction can be understood in terms of internal energy and angular momentum distributions in the metastable species and will be addressed further in the Discussion section.

High-energy collisional activation of $Cl^-(CH_3Br)$ results in formation of approximately equal amounts of Cl^- and Br^- in good agreement with the measurements of Johnson and co-workers.[19] Also observed were $ClBr^-$ and $BrCH_2^-$, which constituted about 1% of the product ions. Dihalide ions have also been reported by Johnson and co-workers in photodissociation studies of several halide–polyhalomethane adduct ions[38] and may arise in the present experiment from collisional excitation of an electron-transfer transition. The $BrCH_2^-$ product ion probably arises from a collisionally activated endothermic proton abstraction reaction.

When the $Br^-(CH_3Cl)$ adduct formed under similar ion source conditions (using CH_2Br_2 as the Br^- precursor) was examined for metastable dissociation, only extremely weak signals of Br^- could be detected. The KERDs for the Br^- formed without added collision gas were again indistinguishable from Br^- formed with added collision gas. Thus, under our experimental conditions, $Br^-(CH_3Cl)$ adducts with lifetimes greater than 10^{-5} s do not undergo unimolecular dissociation to a measurable extent and thus are not metastable. Collisional activation of $Br^-(CH_3Cl)$ yields predominantly Br^- and only a small amount of Cl^- (<5%). The fact that Br^- is not formed by metastable dissociation of the "product complex" $Br^-(CH_3Cl)$, coupled with the very different product ion ratios and energy distributions that result from metastable dissociation vs collisional activation of the reactant and product complexes, provides conclusive evidence that the Br^- we observe from dissociation of $Cl^-(CH_3Br)$ arises only from metastable unimolecular dissociation of the *reactant* complex.

For $Br^-(CH_3I)$, the reactant complex for reaction 3, metastable dissociation yields only the I^- displacement product in our experiments. The KERD for the substitution products is shown in Figure 3. The average relative kinetic energy of the products was about 23 meV. The Br^- product of cleavage of the electrostatic cluster bond was not detected as a product of dissociation on the metastable time scale.

$$Br^- + CH_3I \underset{k_b}{\rightleftarrows} [Br^-(CH_3I)]^* \xrightarrow{k_r} I^- + CH_3Br \qquad (3)$$

The reaction of Cl^- with CH_3I (eq 4) is significantly more exothermic than reactions 2 or 3. Nonetheless, the average kinetic energy release for the $I^- + CH_3Cl$ products was only 24 meV. An inverse isotope effect ($k_H/k_D = 0.84 \pm 0.02$) has been reported for the bimolecular kinetics of this reaction.[37] As shown in Figure 4, the isotope effect on the kinetic energy release distribution is weak. The kinetic energy release distribution for metastable dissociation of $Cl^-(CD_3I)$ is slightly narrower than that for $Cl^-(CH_3I)$. However, the difference is small and may be due to variations in the ion source conditions.

$$Cl^- + CH_3I \underset{k_b}{\rightleftarrows} [Cl^-(CH_3I)]^* \xrightarrow{k_r} I^- + CH_3Cl \qquad (4)$$

The $X^-(CH_3X)$ adducts corresponding to the intermediate complexes in the symmetrical S_N2 reactions (eq 5, with X = Cl,

(38) Cyr, D. M.; Bishea, G. A.; Scarton, M. G.; Johnson, M. A. *Proc. SPIE Int. Soc. Opt. Eng.* **1992**, *74*, 1638.

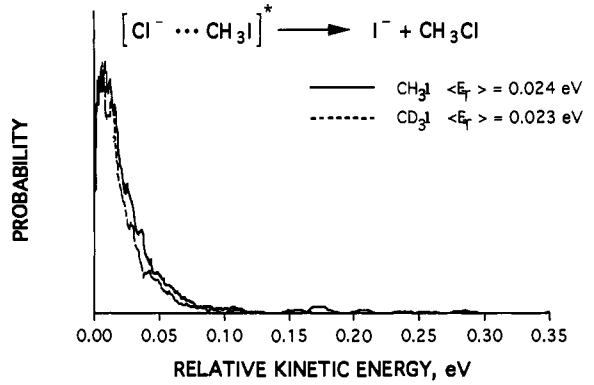

Figure 4. Experimental metastable kinetic energy release distribution for the displacement reactions $Cl^-(CH_3I) \rightarrow I^- + CH_3Cl$ (solid line) and $Cl^-(CD_3I) \rightarrow I^- + CD_3Cl$ (dashed line).

Table 1. S_N2 Barrier Heights Relative to Reactants, $\Delta E^{\ddagger}$, Calculated from Phase Space Modeling of Experimental S_N2 Reaction Kinetics

reactants	k_{expt}[a]	k_{coll}[b]	Φ[c]	$\Delta E^{\ddagger}$,[d] eV
$Cl^- + CH_3Cl$	3.5×10^{-14} [e]	1.88×10^{-9}	2×10^{-5}	$+0.12 \pm 0.01$
$Cl^- + CH_3Br$	2.72×10^{-11} [f]	1.75×10^{-9}	0.016	-0.085 ± 0.015
$Cl^- + CH_3I$	1.66×10^{-10} [f]	1.75×10^{-9}	0.095	-0.20 ± 0.02
$Br^- + CH_3I$	2.89×10^{-11} [f]	1.30×10^{-9}	0.022	-0.11 ± 0.02

[a] Cm^3/molecule-s. [b] Collision rate constant calculated using ADO theory. [c] $\Phi = k_{expt}/k_{coll}$. [d] Details given in the Appendix. [e] Reference 44. [f] Reference 37.

Br, or I) were not observed to undergo metastable dissociation.

$$X^- + CH_3X \underset{k_b}{\rightleftarrows} [X^-(CH_3X)]^* \xrightarrow{k_f} X^- + CH_3X \qquad (5)$$

Theoretical Phase Space Calculations. The details of these calculations are given in the Appendix, and only the results will be noted here. The calculations employ the double-well potential shown in Figure 1. The activation energies for the S_N2 reactions were estimated by modeling the bimolecular reaction kinetics at 300 K. We used the values for the thermal energy rate constants obtained recently by Gronert et al.[37] These rate constants are in agreement with earlier measurements of the kinetics for reactions 2 and 3,[7,39-42] and with the recent measurements for reaction 2 by Viggiano and co-workers.[28] The activation energies that result from modeling the kinetics are collected in Table 1. The sensitivity of the calculated kinetics to the vibrational frequencies used for the S_N2 transition states is indicated by the uncertainty in $\Delta E^{\ddagger}$. Also included as a point of comparison is the symmetrical reaction of $Cl^- + CH_3Cl$.[43] The activation energy determined from modeling the bimolecular kinetics with statistical phase space theory corresponds to $\Delta H^{\ddagger}$ at 0 K and is in good agreement with values derived from ab initio calculations by adding zero-point vibrational energy to the calculated $\Delta E^{\ddagger}$. We obtain $\Delta H^{\ddagger} = +2.8$ kcal/mol, as compared to 2.4[14,17] and 3.3 kcal/mol,[15] and a semiempirical value of 1.9 kcal/mol.[15] Our value for the activation energy for reaction of Cl^- with CH_3Br is -2.0 kcal/mol, which is also in good agreement with ab initio results.[44] Using this activation energy, we modeled the temperature dependence for reaction 2. Viggiano and co-workers have measured the temperature dependence of this reaction and were able to separate the effects of kinetic and internal energy.[28]

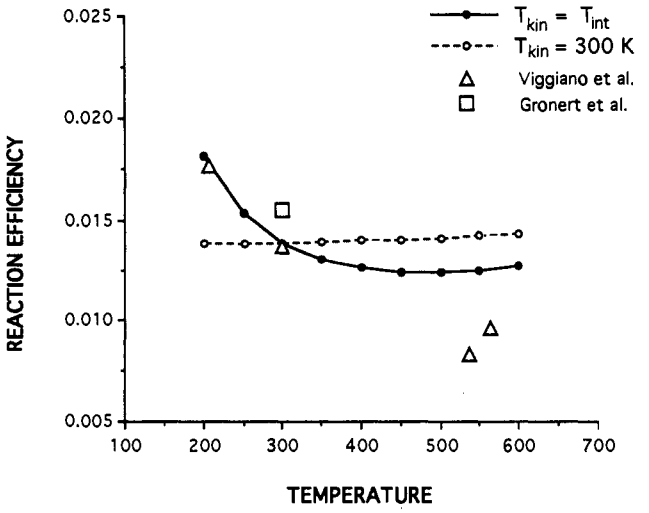

Figure 5. Temperature dependence calculated with phase space theory for the efficiency of the bimolecular displacement reaction $Cl^- + CH_3Br$, for kinetic and internal temperature varied (closed circles), and for kinetic temperature held constant at 300 K and internal temperature varied (open circles). The open triangles are the data of Viggiano et al.,[28] and the open square is the rate constant measured at 300 K by Gronert et al.[37]

For comparison with their data, we calculated total temperature (translational and vibrational) and internal energy (vibrational only) dependence, and the results are shown in Figure 5 as a plot of reaction efficiency versus temperature, where efficiency is defined as the ratio of the experimental rate constant to the collision rate constant (k_{expt}/k_{coll}), with k_{coll} given by ADO theory.[45] The calculation (solid line) reproduces the experimental temperature dependence at low temperatures, but at higher temperatures the calculated efficiencies are greater than the experimental values. To determine the internal energy dependence, the translational temperature in the calculation was held constant at 300 K, while the internal temperature was varied from 200 to 600 K. The results, shown as the dashed lines in Figure 5, show that statistical theory predicts essentially no dependence on internal energy for this temperature range; the temperature dependence is entirely a consequence of kinetic energy effects. As a final test of our activation energies, we attempted to calculate kinetic isotope effects, which have been measured experimentally for reactions 2–4.[37] Depending on the choice of vibrational frequencies for the S_N2 transition state, the predicted kinetic isotope effect k_H/k_D ranged from about 0.6 to near 1. Thus, the calculations predict the inverse isotope effect observed by Gronert et al., but the magnitude of the effect cannot be determined precisely.

Kinetic energy release distributions were calculated for metastable dissociation of the $X^-(CH_3Y)$ species corresponding to the reaction intermediates in eq 2–4, using the method described in the Appendix. The resulting KERDs are shown in Figures 6–8 with the experimental data. In each case, the statistical KERD is significantly broader than the experimental results. This result indicates that less energy is partitioned to relative translation of the dissociation products than is predicted for statistical dissociation; thus the products are internally excited. In order to determine the approximate amount of excess internal energy in the products, we calculated KERDs assuming that varying amounts of the reaction exothermicity were not available for product translation. As expected, as this "fixed" energy increases, the calculated KERDs narrow, but no single KERD can reproduce the experimental results. However, by summing together two or more of these distributions, we can reproduce the experimental data quite well. Shown in Figures 6–8 are

(39) Tanaka, K.; Mackay, G. I.; Payzant, J. D.; Bohme, D. K. *Can. J. Chem.* **1976**, *54*, 1643.
(40) Caldwell, G.; Magnera, T. F.; Kebarle, P. *J. Am. Chem. Soc.* **1984**, *106*, 959.
(41) Ingemann, S.; Nibbering, N. M. M. *Can. J. Chem.* **1984**, *62*, 2293.
(42) Bohme, D. K.; Raksit, A. B. *Can. J. Chem.* **1985**, *63*, 3007.
(43) Barlow, S. E.; Van Doren, J. M.; Bierbaum, V. M. *J. Am. Chem. Soc.* **1988**, *110*, 7240.
(44) Truhlar, D. G., private communication.
(45) Su, T.; Bowers, M. T. In *Gas Phase Ion Chemistry*; Bowers, M. T.; Ed.; Academic Press: New York, 1979; Vol. 1, p 84.

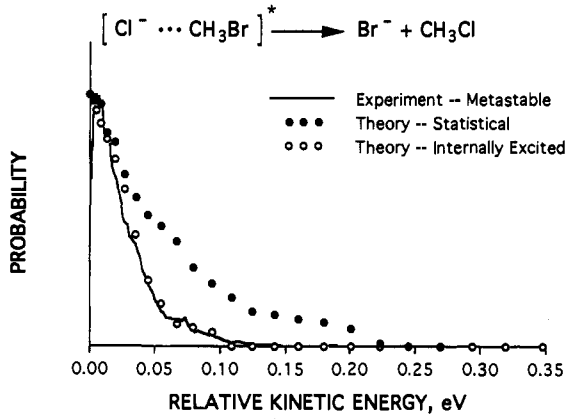

Figure 6. Kinetic energy release distributions for $Cl^-(CH_3Br) \rightarrow Br^- + CH_3Cl$. The solid line is the experimental data and the points are the distributions calculated with phase space theory. The closed circles correspond to the predicted distribution for statistical dissociation with all reaction energy available; the open circles correspond to the predicted distributions if vibrationally excited methyl chloride is formed. (See Table 2.)

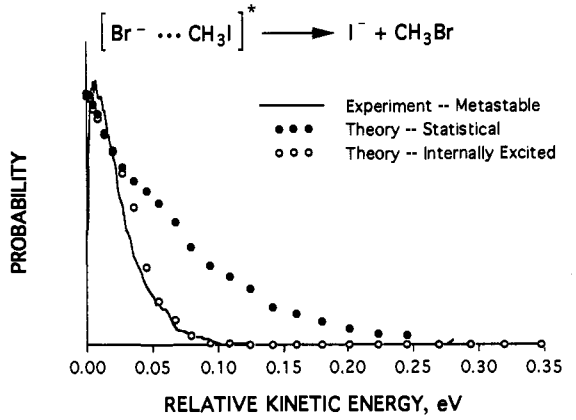

Figure 7. Kinetic energy release distributions for $Br^-(CH_3I) \rightarrow I^- + CH_3Br$. The solid line is the experimental data, and the points are the distributions calculated with phase space theory. The closed circles correspond to the predicted distribution for statistical dissociation with all reaction energy available; the open circles correspond to the predicted distributions if vibrationally excited methyl bromide is formed. (See Table 2.)

distributions that have been determined by a linear-least-squares fit of KERDs calculated for three different fixed energies. In Table 2 the parameters that gave the best fit of the experimental distributions are listed. These parameters should be considered only qualitative indicators of the actual fixed energy, due to the approximations and assumptions inherent to this analysis. For example, these results assume that energy in excess of the fixed energy partitions statistically among translational, vibrational, and rotational modes; *i.e.*, the fixed energy is solely vibrational. This assumption will be addressed further in the Discussion. The fact that the experimental distributions are not reproduced by a single vibrational energy is to be expected; some energy randomization must be occurring for the metastable substitution reaction to occur.

The calculated KERDs are most strongly affected by the total energy released in the reaction and the molecular parameters of the orbiting transition state in the product channel and are relatively insensitive to the parameters used for the reaction complex and the S_N2 transition state. For example, for reaction 2, $\Delta E^\ddagger$ was varied from the optimized value of −2.0 to about −7.0 kcal/mol. This had two effects: the KERDs narrowed slightly, and the lifetimes of the collision complexes shortened dramatically. Because the complex lifetimes were built into the calculation, we generally reached the stage where the calculations predicted that

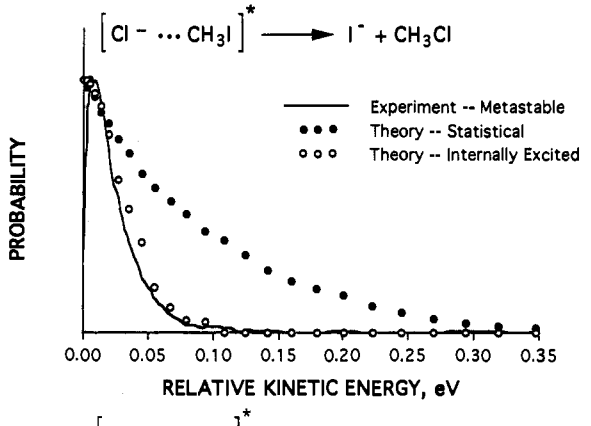

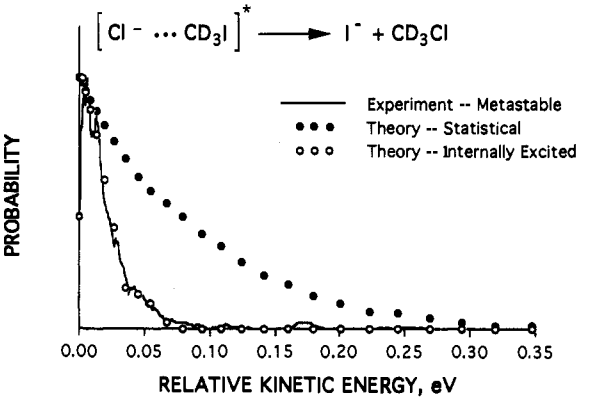

Figure 8. Kinetic energy release distributions for (a) $Cl^-(CH_3I) \rightarrow I^- + CH_3Cl$ and (b) $Cl^-(CD_3I) \rightarrow I^- + CD_3Cl$. The solid line is the experimental data, and the points are the distributions calculated with phase space theory. The closed circles correspond to the predicted distribution for statistical dissociation with all reaction energy available; the open circles correspond to the predicted distributions if vibrationally excited methyl chloride is formed. (See Table 2.)

Table 2. Fixed Vibrational Energies for Calculated KERDs Shown in Figures 6–8

	$Cl^- + CH_3Br$	$Br^- + CH_3I$	$Cl^- + CH_3I$	$Cl^- + CD_3I$
E_{vib}, eV ($P[E_{vib}]$)[a]	0.20 (*0.35*)	0.28 (*0.34*)	0.36 (*0.35*)	0.49 (*0.34*)
	0.18 (*0.33*)	0.22 (*0.33*)	0.35 (*0.34*)	0.43 (*0.34*)
	0.13 (*0.32*)	0.18 (*0.32*)	0.30 (*0.31*)	0.35 (*0.32*)
$\langle E_{vib} \rangle$[b] eV	0.17	0.23	0.34	0.42

[a] Fixed vibrational energies and relative contributions (in parentheses) to fitted KERDs. [b] Average fixed vibrational energy.

the species were no longer metastable (*i.e.*, the lifetimes were significantly less than 10 μs) before the calculated KERD had narrowed significantly. Changes of ±25–50% in the lowest frequency vibrations (<500 cm^{-1}) for the transition state and the complex resulted in fairly significant changes in the kinetics and complex lifetimes, respectively, but had essentially no effect on the calculated KERDs.

The fact that the complexes we are studying may have undergone stabilizing collisions in the ion source leads to some uncertainty in the internal energy and total angular momentum distribution P(E,*J*) of the metastable complexes. From the statistical phase space calculations, we find that complexes with energies only slightly greater than the cluster binding energy should have lifetimes shorter than the 10 μs time scale of this experiment. To account for the possibility of partial collisional stabilization, the energy distributions used for reactant complex in the calculations were extended to include internal energies less than the complex bond energy. This was also necessary to calculate a significant probability of metastable dissociation. However, the shape of the internal energy distributions used in the calculations had little effect on the predicted KERD. Similarly, the angular momentum distribution function used had

very little impact on the results of the calculation. This is due mainly to the 10 μs lifetime requirement; only a relatively small set of (E,J) states is calculated to be metastable. The lifetimes we calculate may be underestimated as a consequence of the difficulty in calculating accurate kinetics for dissociation through an orbiting transition state[46] or because the state-counting algorithm neglects anharmonicity of the vibrations (or because the dissociation dynamics are nonstatistical). However, if parameters are modified in order to increase the calculated complex lifetimes by one or two orders of magnitude, the effect is to broaden the KERDs slightly rather than narrow them. Only by reducing the amount of energy available for partitioning between internal and translational energy in the dissociating species can we achieve narrow calculated KERDs.

Discussion

In a series of trajectory calculations investigating the dynamics of the symmetrical S_N2 reaction $Cl^- + CH_3Cl$ (eq 5, X = Cl), Vande Linde and Hase have uncovered features such as vibrational mode-selective rate enhancement and multiple crossings of the transition state dividing surface,[24,25,27] which are clearly inconsistent with the basic assumptions of statistical models. What is less clear, however, is how such features will be manifest in the overall kinetics of the reaction. One of the goals in modeling reaction kinetics with statistical theory is to obtain information about the potential energy surface, viz. activation energies and/or thermochemistry. This is often accomplished by assuming the reaction intermediate is at steady state and relating the efficiency of the bimolecular reaction, defined as k_{expt}/k_{coll}, to the branching ratio $k_f/(k_f + k_b)$ for unimolecular dissociation of the intermediate (eq 6).

$$X^- + CH_3Y \xrightarrow{k_{expt}} Y^- + CH_3X$$

$$X^- + CH_3Y \underset{k_b}{\overset{k_{coll}}{\rightleftarrows}} [X^- \cdots CH_3Y]^* \xrightarrow{k_f} Y^- + CH_3X \qquad (6)$$

The branching ratio for unimolecular dissociation of the intermediate can then be modeled as a unimolecular reaction using statistical theory. For S_N2 reactions, the various elements of the nonstatistical dynamics observed by Vande Linde and Hase can have opposing influences on the value of the transition-state energy determined from statistical theory. That is, dynamical bottlenecks in complex formation decrease the effective capture collision rate constant k_{coll} relative to the collision theory. If this is not taken into account in the model, the calculated transition-state energy may be too high. Compounding this effect would be multiple crossings of the transition-state dividing surface, neglect of which can lead to overestimation of the calculated value of k_f, and thus again to a high transition-state energy. However, the possibility of the reaction proceeding in part by a direct mechanism can mitigate these other two effects, by increasing k_{expt} but not k_{coll}.

These points made, it is interesting to note that the activation energies for the reaction of Cl^- with CH_3Cl and CH_3Br as determined by modeling the bimolecular kinetics with statistical phase space theory are in very good agreement with high-level ab initio theory.[14,15,17] Both the experimentally observed inverse deuterium isotope effects[37] and the temperature dependence of the rate constant for eq 2[28] are reproduced qualitatively in the phase space model. There are (at least) two different conclusions that could be drawn from this agreement between experimental kinetics and theoretical modeling. One is that the reaction dynamics are in fact essentially statistical on the reactant side of the barrier and that nonstatistical effects are seen only in those complexes that cross the S_N2 barrier. Alternatively, any nonstatistical effects that do operate cancel each other out overall, as discussed above. In either case, these results suggest that, in spite of recent reports of nonstatistical dynamics for these reactions, the use of statistical theory to characterize the gross features of the potential energy surfaces of gas-phase S_N2 reactions (such as activation energies) is not yet contraindicated.

A more central issue in this paper is the disposal of the released reaction energy in the products of the substitution reactions. Our results show average translational energies of the S_N2 products that are much less than predicted by statistical theory, which leads to the conclusion that the released energy is largely sequestered in internal modes of the neutral methyl halide product. We successfully modeled this phenomenon by assuming that a certain amount of the *vibrational* energy in the reactant complex was not available for randomization, and thus that the methyl halide products were vibrationally excited, but that the rotational distributions were statistical (Figures 6–8). We now address the possibility of a nonstatistical *rotational* distribution.

The S_N2 mechanism for unsubstituted methyl halides, such as those in the present study, is viewed as proceeding via a transition state of C_{3v} symmetry.[47] In such a system, one might expect that the products will separate with very little rotational excitation, the dipole of the neutral molecule being optimally aligned with the departing anion. Because of the requirement of conservation of angular momentum in the overall reaction, low rotational excitation in the products would have to be balanced by high orbital angular momentum in the separating products, which would appear in our experiments as translational energy. From this simple view of the mechanism, a broader-than-statistical translational energy distribution would be predicted, and not the narrow distribution observed. Thus, while we cannot rule out the possibility of a nonstatistical rotational distribution, it seems unlikely to be responsible for the narrow experimental KERDs.

Vibrational excitation in the products of S_N2 reactions has been predicted previously[21] and may be rationalized in terms of the recent trajectory calculations of Vande Linde and Hase, which suggest that the low-frequency "intermolecular" vibrational modes (the X–C–Y bend and stretch modes) of the reaction or product complexes are only weakly coupled to the "intramolecular" modes of the CH_3Y or CH_3X moiety. The S_N2 transition state incorporates a CH_3X moiety that is strongly distorted relative to the geometry of the isolated methyl halide product. If the vibrational energy associated with this distorted geometry remains largely sequestered in the nascent CH_3X even within the product complex, little energy will be available for relative translation of the Y^- and CH_3X products. What this amounts to is slow v–v transfer (intramolecular to intermolecular modes) followed by rapid dissociation of the C–Y electrostatic bond as the energy transferred into the asymmetric X–C–Y stretch reaches the dissociation limit. A similar mechanism has been proposed for photodissociation of $CO_3^-(H_2O)$ and $CO_3^-(CO_2)$, which may involve as sequential intermediate states an electronically excited state and a vibrationally excited ground state localized on the CO_3^- moiety.[48]

The parameters for the calculated distributions that best fit the experimental data are listed in Table 2. A brief consideration of these results can help to illustrate how substantial the effect is. In the case of the reaction of Cl^- with CH_3Br, the overall reaction (eq 2) is exothermic by 0.29 eV. As shown in Table 2, the average energy unavailable for randomization in the $Br^- + CH_3Cl$ products is 0.17 eV, or more than half of the energy released in the reaction. This average energy is approximately the energy of the CH_3Cl methyl umbrella mode (1355 cm^{-1}, 0.17 eV). The data are best fit by a combination of three calculated distributions, with the fixed vibrational energies 0.13, 0.18, and 0.20 eV. These

(46) Chesnavich, W. J.; Bass, L. M.; Su, T.; Bowers, M. T. *J. Chem. Phys.* **1981**, *74*, 2228.

(47) Ingold, C. K. *Structure and Mechanism in Organic Chemistry*, 2nd ed.; Cornell University Press: Ithaca, NY, 1969.

(48) Snodgrass, J. P.; Kim, H.-S.; Bowers, M. T. *J. Chem. Phys.* **1988**, *88*, 3072.

could be associated respectively with one quantum in the methyl wag (1017 cm^{-1}, 0.13 eV), two quanta in the C–Cl stretch (732 cm^{-1}, 0.091 eV), and one quantum in either the methyl umbrella mode or the asymmetric methyl deformation (1452 cm^{-1}, 0.18 eV). While this interpretation is not intended to serve as an assignment, it does show that the amount of fixed vibrational energy that results from our analysis is reasonable.

For the other reactions studied, we consider only the average fixed vibrational energy. The reaction of Br^- with CH_3I is exothermic by 0.36 eV, and the average fixed energy in the I^- + CH_3Br products is about 0.23 eV. This energy is approximately equal to a combination of one quantum in the C–Br stretch (611 cm^{-1}, 0.076 eV) plus one quantum in the methyl umbrella mode (1306 cm^{-1}, 0.16 eV). In the Cl^- + CH_3I reaction (0.59 eV exothermic), 0.34 eV is unavailable for randomization in the I^- + CH_3Cl products. This energy is approximately that of two quanta in the CH_3Cl methyl umbrella mode (0.34 eV) or one quantum in that mode plus two in the C–Cl stretch (0.35 eV). In the reaction of Cl^- with CD_3I, the average fixed energy of 0.42 eV could be associated with several different combinations of excited vibrational modes, including two quanta CD_3 umbrella plus two quanta C–Cl stretch (0.43 eV). Again, these are not intended as assignments but rather to demonstrate that the results are consistent with vibrational frequencies in the products.

A question that arises at this stage is whether our results can be related to the bimolecular S_N2 reaction. Our calculations predict that, at only a few tenths of an eV above the dissociation thresholds, the lifetimes of the intermediate complexes are typically much shorter than the 10 μs required for detection in the metastable experiments. As a consequence, the distribution of internal energy in the metastable complexes is very narrow. Because of this limited energy, only those metastable complexes with relatively low total angular momentum can pass the S_N2 transition state and form products. Thus, the internal energy and angular momentum distributions in the relatively long-lived metastable complexes are quite different from those in the nascent collision complexes. We expect, however, that the kinetic energy distributions for the products of the bimolecular reactions will be similar to our metastable results, at least for the portion of the reaction that proceeds through a complex. This conclusion is based on the similarity of the results for the mildly exothermic Cl^- + CH_3Br reaction and the more exothermic Cl^- + CH_3I reaction, which demonstrates that even when more reaction energy is available to the dissociating species, the partitioning of that energy nonetheless favors translationally cold and internally hot products.

In this context, the apparent discrepancy between our metastable results and the kinetic energy ICR studies of Buckner and co-workers is puzzling.[33] They observe enhanced translational energy releases (and, by inference, cold internal energy distributions) for the reaction of F^- with CH_3Cl. We were unable to examine this reaction in the metastable realm due to difficulties in generating the intermediate complex. It is possible that this reaction is intrinsically different from the ones we studied; it is considerably more efficient and consequently is expected to have a much lower activation energy.[49] For example, the F^- + CH_3Cl reaction may proceed essentially exclusively by a direct mechanism, which may exhibit very different dynamics from complex-mediated reactions. For the time being, we are unable to resolve this issue; clearly, further studies are warranted.

Conclusions

We have studied the deposition of reaction energy in products of several gas-phase substitution reactions (X^- + CH_3Y). These reactions have been investigated by means of analysis of product relative kinetic energy distributions for metastable dissociation of $X^-(CH_3Y)$ adduct species. These adducts are treated as models for the bimolecular reaction intermediates. For this analysis, the bimolecular substitution kinetics have been modeled with statistical phase space theory in order to estimate the activation energies, and the results are in good agreement with high-level ab initio calculations, where available. For the reaction of Cl^- with CH_3Br, both the experimental kinetic isotope effect and the temperature dependence are reproduced qualitatively by the phase space calculations. The calculations predict different effects on bimolecular substitution reaction kinetics for internal CH_3Br (vibrational) energy vs total (relative kinetic + internal) energy, as has been observed experimentally by Viggiano and co-workers. The results indicate that, in spite of the nonstatistical dynamics predicted for these reactions, the thermal energy kinetics and the S_N2 activation energies are adequately modeled by statistical theories.

Nonstatistical partitioning of the released reaction energy is clearly demonstrated by the results of the metastable dissociation studies, in which the substitution products are formed with significantly less relative translational energy than is predicted by statistical phase space theory. It can be deduced from consideration of the S_N2 mechanism and from modeling of the kinetic energy release distributions that the methylhalide products are vibrationally excited, which is consistent with theoretical predictions for related substitution reactions.

Table 3. Summary of Input Parameters Used in the Phase Space Calculations for Cl^- + CH_3Cl

	Cl^- + CH_3Cl	$[Cl–CH_3–Cl]^\ddagger$
v_i[a] cm^{-1}	3039 (2)	3055 (2)
	2937	2900
	1452 (2)	1320 (2)
	1355	1038
	1017 (2)	1021 (2)
	732	200
		160 (2)
B,[b] cm^{-1}	0.994	0.207
α,[c] $Å^3$	13.3 (4.43)	
σ[d]	3	3
$\Delta\Delta E$,[e] eV	0.0	0.12
μ,[f] amu	20.59	

[a] Vibrational frequencies (degeneracies), estimated as described in text. [b] Geometrical mean rotational constant. [c] Scaled polarizability (see text); value in parentheses is true polarizability. [d] Rotational symmetry number. [e] Energy difference in eV, relative to separated reactants. [f] Reduced mass.

Acknowledgment. We are grateful to Mr. John E. Bushnell for his assistance in the measurement of the KERD data for $Cl^-(CD_3I)$. We also wish to thank Professor Donald G. Truhlar for communicating the results of his calculations for Cl^- + CH_3Br and CD_3Br prior to publication and Professor Terry B. MacMahon for supplying experimental data on complex binding energies. This research was supported by a grant from the National Science Foundation (CHE-91-19752) (M.T.B.). S.T.G. acknowledges the U. C. President's Fellowship program for support in the form of a postdoctoral fellowship while at UCSB and the Camille and Henry Dreyfus Foundation for a 1992 New Faculty Award.

Appendix

These reactions are modeled using statistical phase space theory, with the double-well potential shown in Figure 1. Four species enter into the calculations: the two orbiting transition states for association of the reactants and of the products, the reactant complex, and the S_N2 transition state. The parameters used in the calculations are summarized in Tables 3–6. These calculations utilize an effective potential in which zero-point vibrational energies are included. The relative energies of the orbiting transition states are estimated from the heats of formation of the

(49) DePuy, C. H.; Gronert, S.; Mullin, A.; Bierbaum, V. M. *J. Am. Chem. Soc.* **1990**, *112*, 8650.

Table 4. Summary of Input Parameters Used in the Phase Space Calculations for $Cl^- + CH_3Br$ and $Cl^- + CD_3Br$

	reactants $Cl^- + CH_3Br$	complex $Cl^-(CH_3Br)$	transition state $[Cl–CH_3–Br]^*$	products $Br^- + CH_3Cl$	reactants $Cl^- + CD_3Br$	transition state $[Cl–CD_3–Br]^*$
ν_i,[a] cm^{-1}	3056 (2)	3055 (2)	3065 (2)	3039 (2)	2297 (2)	2310 (2)
	2935	2940	2930	2937	2160	2160
	1443 (2)	1430 (2)	1400 (2)	1452 (2)	1056 (2)	1035 (2)
	1306	1240	1080	1355	992	778
	955 (2)	915 (2)	940 (2)	1017 (2)	713 (2)	720 (2)
	611	550	225	732	577	225
		80	200 (2)			190 (2)
		30 (2)				
B,[b] cm^{-1}	0.798	0.152	0.163	0.994	0.558	0.129
α,[c] Å^3	14.3 (5.55)			13.3 (4.43)	14.3 (5.55)	
σ[d]	3	3	3	3	3	3
$\Delta\Delta E$,[e] eV	0.0	–0.5	–0.085	–0.29	0.0	–0.085
μ,[f] amu	25.50			30.62	25.72	

[a] Vibrational frequencies (degeneracies), estimated as described in text. [b] Geometrical mean rotational constant. [c] Scaled polarizability (see text); true value is shown in parentheses. [d] Rotational symmetry number. [e] Energy difference in eV, relative to separated reactants. [f] Reduced mass.

Table 5. Summary of Input Parameters Used in the Phase Space Calculations for $Br^- + CH_3I$ and $Br^- + CD_3I$

	reactants $Br^- + CH_3I$	complex $Br^-(CH_3I)$	transition state $[Br–CH_3–I]^*$	products $I^- + CH_3Br$	reactants $Br^- + CD_3I$	transition state $[Br–CD_3–I]^*$
ν_i,[a] cm^{-1}	3060 (2)	3060 (2)	3060 (2)	3056 (2)	2298 (2)	2310 (2)
	2933	2935	2940	2935	2130	2130
	1436 (2)	1425 (2)	1380 (2)	1443 (2)	1049 (2)	1020 (2)
	1252	1200	1010	1306	951	730
	882 (2)	840 (2)	940 (2)	955 (2)	656 (2)	680 (2)
	533	460	220	611	501	220
		90	200 (2)			190 (2)
		30 (2)				
B,[b] cm^{-1}	0.679	0.089	0.101	0.798	0.473	0.0797
α,[c] Å^3	15.6 (7.89)			14.2 (5.55)	15.6 (7.89)	
σ[d]	3	3	3	3	3	3
$\Delta\Delta E$,[e] eV	0.0	–0.5	–0.11	–0.36	0.0	–0.11
μ,[f] amu	50.76			54.02	51.1	

[a] Vibrational frequencies (degeneracies), estimated as described in text. [b] Geometrical mean rotational constant. [c] Scaled polarizability (see text); true value is shown in parentheses. [d] Rotational symmetry number. [e] Energy difference in eV, relative to separated reactants. [f] Reduced mass.

separated species at 0 K. The energies for the reactant complexes $Cl^-(CH_3Br)$ and $Cl^-(CH_3I)$ relative to the separated reactants are taken as the experimental binding energies,[50–53] and that of $Br^-(CH_3I)$, for which experimental data are not available, is estimated by comparison. For the transition states, the relative energy is determined by modeling the thermal energy bimolecular reaction kinetics, as described below.

Vibrational frequencies for the orbiting transition states are estimated from the experimental values for the neutral methyl halides.[54] Frequencies for the reactant complexes and transition states are estimated based on the trends in the theoretically calculated frequencies for the $Cl^- + CH_3Cl$, $Cl^- + CH_3Br$, and $Cl^- + CD_3Br$ reactions.[15,17,44] The low-frequency vibrations we use for the reactant complexes are less than those from the ab initio calculations. This was necessary in order to obtain reasonable complex lifetimes and may reflect vibrational mode anharmonicities, which are not considered in the state counting algorithm. Since the lowest frequency modes are the most important in determining the density of states and hence the kinetics, the sensitivity of the calculations to the choice of these low frequencies was probed by varying them by ±25–50%, as described in the Results section.

The geometric mean rotational constants for the methyl halide moieties in the orbiting transition states were taken from the literature.[55–61] For the reactant complexes and S_N2 transition states, the structures from ab initio calculations for $Cl^-(CH_3Cl)$ were used to estimate percent changes in bond lengths and angles.

Molecular polarizabilities for the CH_3Y species were taken from the listing of Radzig and Smirnoff.[62] The statistical phase space calculations utilize an isotropic ion-induced dipole potential for the long-range potential. Ion-dipole interactions such as are active in the systems under study are stronger at longer range, and use of the true polarizabilities thus underestimates the interactions. In order to compensate for this, the polarizabilities were scaled to values for which the collision rate constants calculated using the Langevin formula for ion-induced dipoles (eq 7) gave values equal to the ADO formula (eq 8) using the correct polarizability.[45,63] In these two equations, α is the polarizability, μ is the reduced mass, μ_D is the dipole moment, and c is an empirical "locking constant."

$$k = 2\pi e\left(\frac{\alpha}{\mu}\right)^{1/2} \tag{7}$$

$$k = 2\pi e\left(\frac{\alpha}{\mu}\right)^{1/2} + ce\mu_D\left(\frac{8\pi}{\mu k_B T}\right)^{1/2} \tag{8}$$

The parameters used for the orbiting transition states, reactant complexes, and S_N2 transition states are listed in Tables 3–6.

(50) Riveros, J. M.; Breda, A. C.; Blair, L. K. *J. Am. Chem. Soc.* **1973**, *95*, 4066.
(51) Dougherty, R. C.; Roberts, J. D. *Org. Mass Spectrom.* **1974**, *8*, 81.
(52) Larson, J. W.; McMahon, T. B. *J. Phys. Chem.* **1984**, *88*, 1083.
(53) McMahon, T. B., private communication.
(54) Shimanouchi, T. *Tables of Molecular Vibrational Frequencies, Consolidated Volume 1*; National Bureau of Standards: Washington DC, 1972.
(55) Townes, C. H.; Schawlow, A. L. *Microwave Spectroscopy*; McGraw-Hill: New York, 1955.
(56) Barnett, T. L.; Edwards, T. H. *J. Mol. Spec.* **1966**, *20*, 347.
(57) Barnett, T. L.; Edwards, T. H. *J. Mol. Spec.* **1967**, *23*, 302.
(58) Maki, A. G.; Hexter, R. M. *J. Chem. Phys.* **1970**, *53*, 453.
(59) Matsuura, H.; Nagakawa, T.; Overend, J. *J. Chem. Phys.* **1970**, *53*, 2540.
(60) Graner, G. *J. Mol. Spec.* **1981**, *90*, 394.
(61) Anttila, R.; Betrencourt-Stirnemann, C.; Dupré, J. *J. Mol. Spec.* **1983**, *100*, 54.
(62) Radzig, A. A.; Smirnov, B. M. *Reference Data on Atoms, Molecules, and Ions*; Springer-Verlag: Berlin, 1985.
(63) Illies, A. J.; Jarrold, M. F.; Bass, L. M.; Bowers, M. T. *J. Am. Chem. Soc.* **1983**, *105*, 5775.

Table 6. Summary of Input Parameters Used in the Phase Space Calculations for $Cl^- + CH_3I$ and $Cl^- + CD_3I$

	reactants $Cl^- + CH_3I$	complex $Cl^-(CH_3I)$	transition state $[Cl–CH_3–I]^*$	products $I^- + CH_3Cl$
υ_i,[a] cm^{-1}	3060 (2)	3060 (2)	3070 (2)	3039 (2)
	2933	2935	2950	2937
	1436 (2)	1420 (2)	1380 (2)	1452 (2)
	1252	1200	1020	1355
	882 (2)	840 (2)	940 (2)	1017 (2)
	533	460	220	732
		90	200 (2)	
		30 (2)		
B,[b] cm^{-1}	0.679	0.131	0.144	0.994
α,[c] $Å^3$	15.6 (7.89)			13.3 (4.42)
σ[d]	3	3	3	3
$\Delta\Delta E$,[e] eV	0.0	–0.5	–0.20	–0.59
μ,[f] amu	28.08			35.88
	reactants $Cl^- + CD_3I$	complex $Cl^-(CD_3I)$	transition state $[Cl–CD_3–I]^*$	products $I^- + CD_3Cl$
υ_i,[a] cm^{-1}	2298 (2)	2290 (2)	2310 (2)	2283 (2)
	2130	2140	2130	2160
	1049 (2)	1040 (2)	1020 (2)	1060 (2)
	951	890	710	1029
	656 (2)	630 (2)	680 (2)	768 (2)
	501	420	220	701
		70	190 (2)	
		30 (2)		
B,[b] cm^{-1}	0.473	0.104	0.114	0.698
α,[c] $Å^3$	15.6 (7.89)			13.69 (4.43)
σ[d]	3	3	3	3
$\Delta\Delta E$,[e] eV	0.0	–0.5	–0.20	–0.59
μ,[f] amu	28.19			37.39

[a] Vibrational frequencies (degeneracies), estimated as described in text. [b] Geometrical mean rotational constant. [c] Scaled polarizability (see text); true value is shown in parentheses. [d] Rotational symmetry number. [e] Energy difference in eV, relative to separated reactants. [f] Reduced mass.

The calculation of the S_N2 transition state energy assumes that the reactant complex is formed at the ADO capture collision rate[45] and dissociates back to reactants or forms substitution products. In this way, the efficiency of the bimolecular reaction (defined as k_{expt}/k_{ADO}) is related to the ratio of the unimolecular rate constants for dissociation of the reactant complex (see eq 6). The S_N2 transition-state energy is then determined by calculating the relative rates for substitution versus back-dissociation while varying the energy of the S_N2 transition state relative to the reactants (ΔE^*).

Deuterium kinetic isotope effects for the reactions of Cl^- with CL_3Br and CL_3I and of Br^- with CL_3I (L = H, D) were modeled by calculating the reaction efficiencies for the deuterated species using the transition-state energies determined above, corrected for the differences in zero-point vibrational energies. The bimolecular reaction temperature dependence measured by Viggiano and co-workers for the reaction of Cl^- with CH_3Br was modeled by calculating the reaction efficiencies for hypothetical reactions in which the translational temperature T_{trans} was 300 K and the vibrational temperature T_{vib} varied from 200 to 600 K, and for the reactions at $T_{trans} = T_{vib}$, again varied from 200 to 600 K. The rotational temperature of the methyl halide was neglected, because for bimolecular ion–molecule reactions, the total angular momentum distribution is determined primarily by the orbital angular momentum of the two reacting particles.

The transition-state energies were determined relative to the reactants and were then incorporated into the calculations of the metastable KERDs, according to eq 9.

$$P(E_T) = \int_E\int_J P(E + \Delta E_C,J)P_{DISS}(E,J;\Delta t)P_T(E + \Delta E_{rxn},J;E_T)dEdJ \quad (9)$$

In this equation $P(E + \Delta E_C, J)$ is the combined internal energy and total angular momentum distribution for the reactant complex with bond energy ΔE_C, P_{DISS} is the probability that the complex with internal energy $E + \Delta E_C$ will dissociate while it is within the second field-free region, and P_T is the probability that the dissociating species will have translational energy E_T. P_{DISS} is given by eq 10, in which k_{TOT} is the total rate for unimolecular dissociation of the complex to products (k_f) or reactants (k_b), and $w(E,J)$ is the probability that the dissociation forms products.

$$P_{DISS}(E,J;\Delta t) = [\exp(-k_{TOT}(E,J)t_i) - \exp[-k_{TOT}(E,J)t_f)]w(E,J) \quad (10)$$

$$k_{TOT}(E,J) = k_f(E,J) + k_b(E,J)$$

$$w(E,J) = \frac{k_f(E,J)}{k_f(E,J) + k_b(E,J)}$$

For vibrationally excited products, eq 9 is replaced by eq 11. In this equation, P_T is calculated for available energy $E + \Delta E_{rxn} - E_{vib}$, where E_{vib} is the vibrational energy assumed to be fixed in the methyl halide product, and is varied from 0.0 eV to ΔE_{rxn} in increments of 0.01 eV.

$$P(E_T) = \int_E\int_J P(E + \Delta E_C,J)P_{DISS}(E,J;\Delta t)P_T(E + \Delta E_{rxn} = E_{vib},J;E_T)dEdJ \quad (11)$$

For ease of visual comparison with experiment, the kinetic energy release distributions are normalized to have the same maximum value when plotted, rather than the same integrated area. However, when the experimental distributions are fit using the linear-least squares method, the calculated distributions are normalized to have the same integrated areas as the experimental distributions. The fit obtained for a combination of three calculated distributions was adequate in each case to reproduce the experimental distributions satisfactorily. A sample of the best five fits based on minimal residual error was inspected, and typically only small variations in the optimal vibrational energy distributions and relative weights were observed. A representative example was chosen for display in Figures 6–8.